# Laser Heating of Solid Matter by Light-Pressure-Driven Shocks at Ultrarelativistic Intensities

K. U. Akli,[1,2,3] S. B. Hansen,[1] A. J. Kemp,[1] R. R. Freeman,[3,4] F. N. Beg,[4] D. C. Clark,[3] S. D. Chen,[4] D. Hey,[1] S. P. Hatchett,[1] K. Highbarger,[3] E. Giraldez,[2] J. S. Green,[5] G. Gregori,[5,7] K. L. Lancaster,[5] T. Ma,[4] A. J. MacKinnon,[1] P. Norreys,[5] N. Patel,[3] J. Pasley,[5] C. Shearer,[2] R. B. Stephens,[2] C. Stoeckl,[6] M. Storm,[6] W. Theobald,[6] L. D. Van Woerkom,[3] R. Weber,[3] and M. H. Key[1]

[1]*Lawrence Livermore National Laboratory, Livermore, California 94550, USA*
[2]*General Atomics, San Diego, California 92186, USA*
[3]*The Ohio State University, Columbus, Ohio 43210, USA*
[4]*University of California, San Diego, San Diego, California 92093, USA*
[5]*Rutherford Appleton Laboratory, Didcot, Oxon, OX11 0QX, United Kingdom*
[6]*Laboratory for Laser Energetics, Rochester, New York 14623, USA*
[7]*Department of Physics, University of Oxford, Oxford OX1 3PU, United Kingdom*

(Received 4 August 2007; published 23 April 2008)

The heating of solid targets irradiated by $5 \times 10^{20}$ W cm$^{-2}$, 0.8 ps, 1.05 $\mu$m wavelength laser light is studied by x-ray spectroscopy of the $K$-shell emission from thin layers of Ni, Mo, and V. A surface layer is heated to ~5 keV with an axial temperature gradient of 0.6 $\mu$m scale length. Images of Ni Ly$_\alpha$ show the hot region has $\leq 25$ $\mu$m diameter. These data are consistent with collisional particle-in-cell simulations using preformed plasma density profiles from hydrodynamic modeling which show that the >100 G bar light pressure compresses the preformed plasma and drives a shock into the solid, heating a thin layer.

DOI: 10.1103/PhysRevLett.100.165002 PACS numbers: 52.38.−r, 52.50.Lp, 52.57.Kk

Intense laser-matter interactions involve novel basic science and have applications including sources of hard x rays for probing high energy density matter [1], collimated proton plasma jets [2], and fast ignition of inertial confinement fusion [3]. Understanding absorption of laser radiation at high intensities, production of MeV electrons, and energy transport with associated isochoric heating is crucial to the development of these applications. The formation of a hot surface layer by sub ps laser irradiation at intensities $>10^{19}$ W cm$^{-2}$ has been reported elsewhere [4,5]. At such high intensities, the collisional range of the MeV electrons produced by absorption of the laser radiation is more than 2 orders of magnitude greater than the thickness of the heated layer and we are concerned with explaining the physics of this heating.

In this Letter, we report a detailed study of hot surface layer formation at a peak intensity of $5 \times 10^{20}$ W cm$^{-2}$ using $K$- shell spectroscopy, monochromatic imaging, and 2D PIC and radiation hydrodynamic modeling of high pressure shock waves. We conclude that our experiment is in a regime of pulse duration and intensity where the light pressure sweeps up the preformed plasma and drives a shock into the solid causing the heating of a thin layer. We also consider the implications for fast ignition [6].

The experiments used the Vulcan laser system at the Rutherford Appleton Laboratory [7]. The laser pulse had a wavelength of 1.05 $\mu$m, 0.8 ps duration, 400 J energy and a peak intensity of $5 \times 10^{20}$ W cm$^{-2}$. An $f/3$ off-axis parabola focused the beam to 7 $\mu$m diameter at half peak intensity with ~30% of the energy in a 15 $\mu$m diameter and the remaining energy distributed over lower intensity wings. The amplified spontaneous emission (ASE) contrast ratio was $4 \times 10^{-8}$ in intensity with a duration of ~2 ns [8]. The targets were 400 $\mu$m × 400 $\mu$m × 5 $\mu$m square foils of Mo with two thin tracer layers: a 0.5 $\mu$m thick Ni layer located at the irradiated (front) surface or under various depths of Mo and a 1 $\mu$m thick V layer located at the rear surface.

A spherically bent Bragg crystal imager [9,10] recorded 2D spatially resolved Ni Ly$_\alpha$ (8.07 keV) images. The full width at half maximum (FWHM) of the images was 25 $\mu$m. This is close to the instrumental spread function and indicates that the highest temperatures are confined radially to $\leq 25$ $\mu$m diameter (Fig. 1).

Two highly ordered pyrolytic graphite (HOPG) crystal spectrometers [11] were used to record spectra from the front and rear sides of the target. Each HOPG had two channels: one channel was angled for the Ni spectrum, the other channel was optimized for V. The spectra were recorded on an image plate detector. Ni $K$-shell x-ray

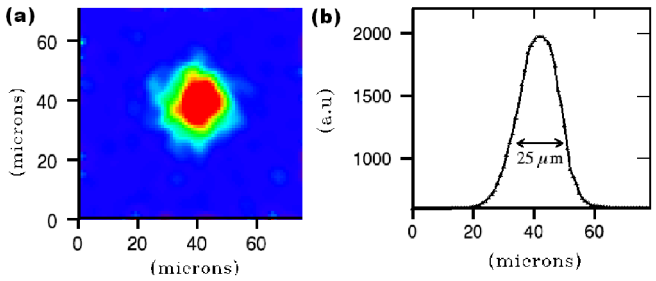


FIG. 1 (color online). (a) Ni Ly$_\alpha$ image of the target with a 0.5 $\mu$m Mo overlay (b) a lineout showing a 25 $\mu$m FWHM.

 

spectra were recorded for targets with the Ni layer on the surface or buried below Mo layers of 0.5, 1.0 or 2.5 $\mu$m thickness. The spectra from Ni at depths up to 1 $\mu$m are shown in Fig. 2(a). The Ni Ly$_\alpha$ (8.07 keV) and He$_\alpha$ (7.76 keV) emission lines are intense when the Ni layer is on the front surface, have sharply reduced intensity with any Mo overlay, and are practically eliminated for Mo thicknesses of 1 $\mu$m and greater, giving direct experimental evidence that the highest temperatures are in a surface layer $<1$ $\mu$m thick. The cold $K_\alpha$ (7.48 keV) emission of Ni is observed for all Ni layer depths. The relative intensities from rear and front HOPGs were normalized using the fact that Ni $K_\alpha$ emission is optically thin. The absolute $K_\alpha$ intensity was determined by calibrating the HOPGs against absolute data from a single photon counting spectrometer [4]. The absolute $K_\alpha$ yield was $4.4 \times 10^{10}$ ph/J accurate to within a factor of 2.4. Vanadium spectra showed cold $K_\alpha$ and $K_\beta$ but no thermal lines, suggesting that the rear-side temperature of the target was $<400$ eV.

We have used synthetic Ni spectra generated by the collisional-radiative model SCRAM [12] to diagnose the plasma conditions. Data from the flexible atomic code (FAC) [13] for neutral to H-like Ni was used to construct a complete and accurate set of levels and rate data based on fine-structure/unresolved transition array (UTA) hybrid level structure [12]. The hot electron fraction in the solid target was estimated to be $<1\%$, based on an upper-limit conversion efficiency of laser light of 50% [14] and a 70 $\mu$m hot electron injection area corresponding to the $K_\alpha$ spot diameter measured on thin Cu targets in this experiment. Although the hot electrons dominate the cold $K_\alpha$ production, their number density is too small to have a significant effect on the ionization balance at solid densities. The calculations are relatively insensitive to the hot electron temperature [15], which was estimated to be 1 MeV from the laser intensity pattern in the focal spot and the pondermotive potential.

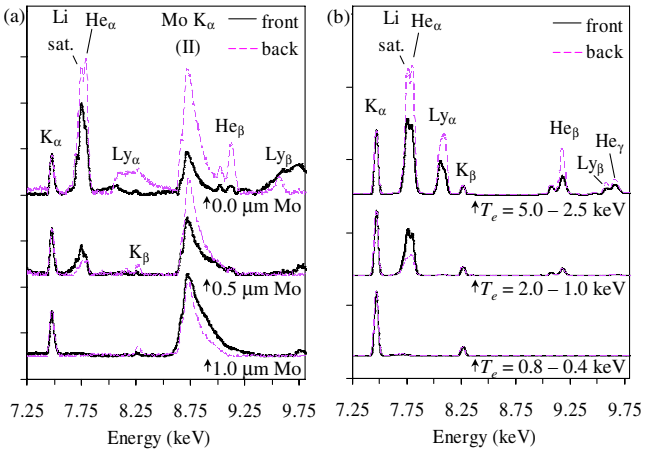


FIG. 2 (color online). (a) Experimental spectra from the front and rear side of 0.5 $\mu$m Ni layers buried under various Mo layer depths (Mo $K\alpha$ in 2nd order is at 8.75 keV). (b) Modeled spectra of Ni layers at various depths with temperature and density profiles discussed in the text (Mo was not modeled).

To determine the characteristics of the heated region, we calculated steady-state spectra for slices of the target corresponding to 1/5 of the total Ni layer at various temperatures and densities. Within each 0.1 $\mu$m slice, the escape factor formalism was used to estimate self-consistent opacity effects and the emissivity ($\varepsilon$) and opacity ($\kappa$) along the line of sight of the HOPG were calculated. Using this set of $\varepsilon(T, \rho, \nu)$ and $\kappa(T, \rho, \nu)$, we found consistent temperature and density profiles that reproduce the major features of the experimental emission spectra after including the effects of transport through neighboring Ni layers and instrumental broadening ($E/\Delta E = 200$). The best-fit synthetic spectra given in Fig. 2(b) reflect the unambiguous experimental evidence for a thin hot surface layer. The He$_\alpha$, He$_\beta$, Ly$_\alpha$, and Ly$_\beta$ emission from the rear HOPG spectrum of the targets with 0.0 and 0.5 $\mu$m Mo layers can be simultaneously fit by a hot layer with a maximum temperature of 5 keV and an $e$-folding length of 0.6 $\mu$m, giving a temperature which decays rapidly from 5 keV in the first 0.1 $\mu$m of the target to 2 keV at a depth of 0.5 $\mu$m and finally to $<600$ eV at a depth of 1.3 $\mu$m. The Ly$_\beta$ to He$_\beta$ lines were favored for this determination because the measured Ly$_\alpha$ line was compromised by the joint in the HOPG crystal; more recent measurements without the joint show a narrower Ly$_\alpha$ feature that resembles the modeled spectra.

If the heated region remained solid, the emission recorded on the rear HOPG would be attenuated along its path through cooler, more opaque material. We find that rear-side emission is indeed less intense than the frontside emission when Ni is buried under 0.5 $\mu$m of Mo. But when the Ni is on the target surface, the reverse is seen: the rear-side He$_\alpha$ is more intense than the frontside emission. We attribute this to expansion of the target in a blow-off region in which the opacity increases with the decreasing collisionality. We can fit the He$_\alpha$ emission from both the front and rear HOPG instruments with a modeled expansion of the first 0.1 $\mu$m of the target from solid to a density of 0.2 g/cm$^3$, the second to 1 g/cm$^3$, and the third to 5 g/cm$^3$, with the remainder of the target at solid density (8.91 g/cm$^3$).

These temperature and density gradients may be not be unique; they are the simplest set of consistent profiles that describe the gross features of the experimental data from all four buried layer depths simultaneously. In particular, the cooling associated with hydrodynamic expansion could amplify the effect of opacity through the expanded surface layers, thereby decreasing the required expansion. Most of the ionization probably occurs at near-solid density during the laser pulse, where ionization time scales between He-like and H-like Ni are on the order of 0.1 ps, rather than in an expanded region where time scales increase inversely with density.

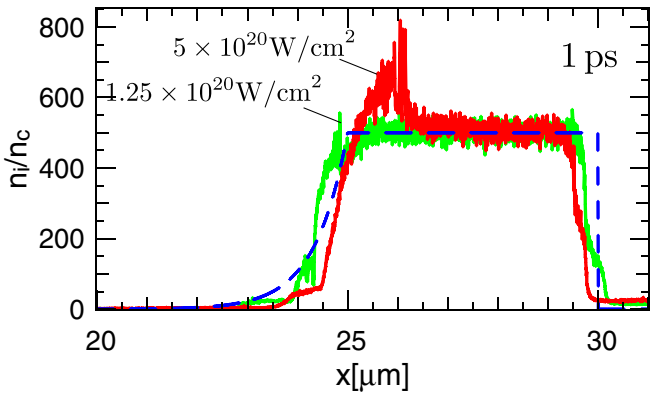


FIG. 3 (color online). Results of 1D PIC simulation-ion density profile at time 1 ps, i.e., after the laser pulse, for two different laser intensities as indicated in the image. Also shown is the initial ion density profile.

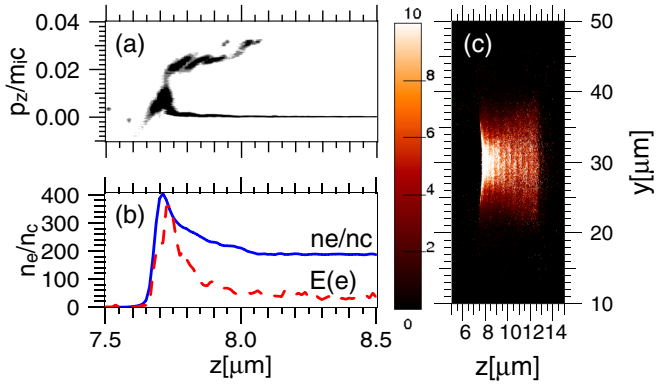


FIG. 4 (color online). Results of 2D PIC simulation—(a) longitudinal ion phase space, (b) electron density (solid line) and energy density (dash-dotted line) along laser irradiation axis; averaged over 0.25 $\mu$m, (c) electron energy density (arbitrary units).

Hydrodynamic modeling of the prepulse from the same laser system indicates that the preplasma extends 2–3 $\mu$m between critical and solid density [4]. Based on this model, we have run a series of 1D particle-in-cell (PIC) simulations of 5 $\mu$m solid density $Mo^{+5}$ slab targets with preplasma at a variety of scale lengths, laser intensities and pulse lengths. Figure 3 shows profiles of the ion density for two cases with 5 $\mu$m of preplasma at a scale length of 0.65 $\mu$m and Gaussian laser pulses with 0.8 ps FWHM, $\lambda = 1$ $\mu$m, at 1 ps. While a pulse with maximum intensity $I_{\max} = 5 \times 10^{20}$ W cm$^{-2}$ is able to sweep up the preplasma and compress a thin layer of solid material, it fails to do so at 4 times reduced intensity. In separate runs we found that 2 times reduced pulse duration also leads to no compression of the solid. Analytic estimates using a self-regulating collisional absorption model [16] and the above hydrodynamic simulations show that the maximum penetration by ASE ablation at the center of the focal spot is $<1/3$ of the 0.5 $\mu$m Ni layer thickness.

Details of the heating process are studied with additional 2D collisional PIC simulations [17] at an intensity $5 \times 10^{20}$ W cm$^{-2}$ with zero rise time and an electron density of $2 \times 10^{23}$ cm$^{-3}$ with no preplasma. These simplifications have been introduced in order to keep the problem computationally tractable. The laser focal spot is Gaussian in space (10 $\mu$m FWHM). The simulation box has a total size of 30 $\mu$m $\times$ 60 $\mu$m at a resolution of 80 cells per $\mu$m and 10 ions plus 50 electrons per cell. Ionization and radiation are ignored. The box has periodic boundary conditions in the transverse direction. Figure 4(a) and 4(b) shows central line-outs of our 2D simulation, i.e., longitudinal ion phase space, electron number density, and electron energy density $\int[\gamma(p) - 1]m_e c^2 f(p) d^3 p$. Figure 4(c) shows the electron energy density in two dimensions. Note that most of the energy is confined to the laser spot region, while hot electrons are present throughout most of the target. Strong heating occurs only over the first 0.3 $\mu$m in the solid. The longitudinal ion phase space shows the signature of a light pressure-driven ion shock [18–20] with a group of ions moving at the flow velocity (0.015 c) behind the shock and a smaller group of reflected ions at twice that velocity. The electron number density shows the compression by the shock. On top of that we have plotted a line out of the energy density from the center of Fig. 4(c). The fact that this quantity increases by more than an order of magnitude in the shock, while particle density increases twofold, illustrates that the material is heated and compressed at the same time.

A simple estimate of the shock heating can be obtained from the Rankine-Hugoniot equations in the strong shock limit taking the shock pressure to be light pressure $\leq I/c$, i.e. 150 G bar at $5 \times 10^{20}$ W cm$^{-2}$, for a small absorption fraction. The specific thermal and kinetic energies behind the shock are then equal at 3.8 erg/g. The SESAME equation of state (EOS) [21] gives a temperature of 6 keV at 3.8 erg/g which is consistent with the experimental temperature. The distance of 1 $\mu$m that the shock travels during the laser pulse is also consistent with the thickness of the heated layer. More accurate modeling with the radiation hydrodynamic code Lasnex [22] also using the SESAME EOS, showed that radiation cooling enhances the compression and reduces the temperature behind the shock, the effects increasing with time and giving after 1 ps a temperature of 5 keV consistent with the experimental data.

We also considered whether Ohmic heating by the return current could explain the data using a 1D numerical model described in Ref. [10]. The model uses the SESAME EOS and the plasma resistivity is classical (Spitzer) but constant below 100 eV to approximate the broad peak in resistivity in the nonclassical regime. It showed that, in order to heat the target to 5 keV, the density must be $<0.06$ g/cm$^3$. Assuming a steep density gradient due to preformed plasma, the heated layer would be thin but the

$<0.06$ g/cm$^3$ density is much too low to allow the production of $Ly_\alpha$ emission during the cooling time of the hot layer. The model also showed heating of the bulk of the target at constant density to temperatures of 250 eV with a scale length $>10$ $\mu$m.

An alternative explanation of heating due to scattering of cold electron return current by magnetic perturbations was given by Sentoku *et al.* based on 3D PIC simulations [23]. We cannot, however, apply this simulation to describe our experimental conditions since it assumed a density 200 times smaller, laser intensity 25 times lower and duration an order of magnitude less than our pulse duration.

The hot surface layer is of intrinsic interest for high energy density science. The experimentally determined diameter of the hot region and its thickness suggest that its thermal energy is however about 0.6 J or 0.3% of the laser energy incident on target. It would be a problem for fast ignition if a significant fraction of the energy were trapped at the surface of a solid target but this is not so. At least 10% of the laser energy is delivered as heat to the bulk of thin targets by hot electrons that are not confined to the surface layer. This has been shown on similar low mass targets using the absolute yield of $K$-shell emission [4] and neglecting energy to fast ions. Ion acceleration in thin targets is evidenced by measurements showing a reduction of the absolute $K$-shell emission yield with decreasing target thickness [10]. Our thin target data are therefore not inconsistent with earlier estimates of $>30\%$ conversion to hot electrons at the intensities of this work [14], which is important for fast ignition. Another consequence of the steepening of the density gradient predicted by PIC modeling is reduced hot electron temperature [24]. This effect could be highly advantageous for electron fast ignition by avoiding the production of higher than required hot electron temperature [6].

In conclusion, heating of a thin layer at near-solid density to 5 keV temperature by $5 \times 10^{20}$ W cm$^{-2}$ laser irradiation is attributed to the light-pressure-driven shock. Such shock heating is expected only when light pressure and pulse duration are sufficient to sweep up preformed plasma, conditions which are shown to be reached in this experiment and would be more strongly in effect for full scale fast ignition where pulse durations would be 20 ps at intensities similar to those in this work. The heating is interesting in its own right for creation of high energy density states of matter. It is not a major drain of electron energy and therefore does not adversely affect fast ignition.

We acknowledge useful discussions with H. Ruhl, Y. Sentoku, and P. K. Patel and use of Vulcan laser and PSC code. This work was performed under the auspices of the U.S. Department of Energy by the Lawrence Livermore National Laboratory under Contract No. W-7405-ENG-48.

[1] O. L. Landen *et al.*, Rev. Sci. Instrum. **72**, 627 (2001).
[2] R. Snavely *et al.*, Phys. Rev. Lett. **85**, 2945 (2000).
[3] M. Tabak *et al.*, Phys. Plasmas **1**, 1626 (1994).
[4] W. Theobald *et al.*, Phys. Plasmas **13**, 043102 (2006).
[5] H. Nishimura *et al.*, Plasma Phys. Controlled Fusion **47**, B823 (2005).
[6] M. H. Key, Phys. Plasmas **14**, 055502 (2007).
[7] C. N. Danson *et al.*, Proc. SPIE Int. Soc. Opt. Eng. **3047**, 505 (1997).
[8] I. Musgrave *et al.*, Appl. Opt. **46**, 6978 (2007).
[9] J. Koch *et al.*, Rev. Sci. Instrum. **74**, 2130 (2003).
[10] K. U. Akli *et al.*, Phys. Plasmas **14**, 023102 (2007).
[11] S. Glenzer *et al.*, Phys. Plasmas **10**, 2433 (2003).
[12] S. B. Hansen *et al.*, High Energy Density Phys. **3**, 109 (2007).
[13] M. F. Gu, Astrophys. J. **590**, 1131 (2003).
[14] K. Yasuike *et al.*, Rev. Sci. Instrum. **72**, 1236 (2001).
[15] S. B. Hansen *et al.*, Phys. Rev. E **70**, 036402 (2004).
[16] M. H. Key, *Handbook of Plasma Physics*, Vol. 3 (Elsevier, Amsterdam, 1991), p. 575.
[17] H. Ruhl, *Introduction to Computational Methods in Many Body Physics* (Rinton Press, Princeton, New Jersey, 2005).
[18] L. O. Silva *et al.*, Phys. Rev. Lett. **92**, 015002 (2004).
[19] J. Denavit, Phys. Rev. Lett. **69**, 3052 (1992).
[20] S. Miyamoto *et al.*, J. Plasma Fusion Res. **73**, 343 (1997).
[21] S. P. Lyon and J. D. Johnson, The Los Alamos National Laboratory EOS Database Report No. LA-UR-92-3407, 1992.
[22] G. B. Zimmerman and W. L. Kruer, Comments Plasma Phys. Control. Fusion **2**, 51 (1975).
[23] Y. Sentoku *et al.*, Phys. Rev. Lett. **90**, 155001 (2003).
[24] S. C. Wilks *et al.*, Phys. Rev. Lett. **69**, 1383 (1992).